Polar organic contaminants in natural drinking water sources and their removal by reverse osmosis

A high-resolution mass spectrometry study

Albergamo, V.

Publication date
2019

Document Version
Other version

License
Other

Chapter 4. Removal of polar organic micropollutants by mixed-matrix reverse osmosis membranes

Abstract

To produce high-quality drinking water, reverse osmosis (RO) membranes with mixed-matrix active layers have been proposed to outperform standard polyamide thin-film composite (TFC) membranes. We investigated the passage of 30 persistent polar micropollutants (MPs) in a pilot-scale RO system equipped with a 4-inch zeolite-embedded thin-film nanocomposite (TFN) membrane and fed with raw riverbank filtrate. Additionally, MPs passage was investigated in a bench-scale system equipped with a 1.8-inch aquaporin-embedded RO membrane. Benchmark TFC membranes were used in both systems. In pilot-scale RO, MPs passage did not exceed 15% and 6% with the TFC and TFN membranes, respectively. In bench-scale RO, MPs passage values of up to 65% and 44% were quantified for the aquaporin and TFC membranes, respectively, suggesting a more open structure of the 1.8-inch modules. In both RO systems, uncharged polar MPs displayed the highest passage values. Overall, no statistical differences between passage values were found between TFC and mixed-matrix RO membranes, indicating that nanocomposite and biomimetic membranes are as effective as TFCs of the same module size in preventing breakthrough of polar organics.

4.1. INTRODUCTION

Natural waters are ubiquitously polluted with anthropogenic organic micropollutants (MPs) (Schwarzenbach et al., 2006). Of particular concern for the quality of drinking water sources are the emissions of polar MPs via point and nonpoint sources, *e.g.* domestic wastewater treatment plants effluents (Loos et al., 2009; Luo et al., 2014) and agricultural runoffs (Gray et al., 2017). As polar compounds can preferentially partition into the water phase they can be highly mobile within the water cycle (Reemtsma et al., 2016). If persistent, dissolved MPs can spread to water bodies downstream of their emission sources or accumulate in semi-enclosed aqueous environments. Reports on the link between exposure to trace concentrations of (single) polar MPs and disruption of biological functions of aquatic biota have emerged (Hayes et al., 2010; Kashiwada et al., 2002), raising concern over the adverse effects to human health via insufficiently treated drinking water (Diamanti-Kandarakis et al., 2009; Schriks et al., 2010).

It has been estimated that by 2025 1.8 billion people would inhabit areas affected by water scarcity and about two-thirds of the world's population will live in water-stressed regions as a result of the cumulative effect of water use, population growth, and climate change (FAO, 2007). Advanced water treatment processes relying on osmotic membranes are employed by drinking water utilities to cope with the dramatic increase in clean potable water demand. In particular, reverse osmosis (RO) has shown great potential to remove a wide range of contaminants from a variety of water matrices (Lee et al., 2008; Radjenović et al., 2008). The passage of solutes through RO membranes is assumed to follow the solution-diffusion model, where solutes dissolve into the membrane's active layer, *i.e.* the outermost polymeric layer responsible for solute separation, and diffuse through it along a transmembrane chemical potential gradient (Wang et al., 2014; Wijmans and Baker, 1995). The solution-diffusion process can be promoted or hindered by various mechanisms, *i.e.* size exclusion (Kimura et al., 2003b; Ozaki and Li, 2002), electrostatic attraction or repulsion (Nghiem et al., 2006; Verliefde et al., 2008), and hydrophobic interactions (Kimura et al., 2003a; Verliefde et al., 2009). These mechanisms are in turn influenced by the physicochemical properties of both membrane and solutes, the composition of feed water and operating conditions of RO processes (Bellona et al., 2004; Plakas and Karabelas, 2012).

The most successful RO membranes nowadays are thin-film composite (TFCs) constructed in spiral wound module configuration (Lee et al., 2011; Perreault et al., 2014; Petersen, 1993). A typical TFC membrane consists of three layers, with the outer-most active layer being in contact with the feed

solution and typically consisting of cross-linked aromatic polyamide (PA) obtained by interfacial polymerisation of 1,3-benzenediamine and trimesoyl chloride on top of a polysulfone layer, which is in turn supported by a polyester web. PA active layers are selective for water molecules and provide a high salt rejection, whereas the layers underneath provide support to the overall structure and increase water fluxes to the permeate side as they are more hydrophilic than the active layer (Lee et al., 2011). Despite PA-based TFC membranes have improved over the last decades in terms of water permeability and salt rejection, performance enhancements are limited by the permeability and selectivity trade-off relationship, where an increase in water permeability will necessarily result in increased solute passage (Geise et al., 2011; Werber et al., 2016). State-of-the art low-pressure PA-based TFC membranes serve as reference membranes for any novel material developed for RO filtration (Petersen, 1993). The simplicity of modifying the interfacial polymerisation process has allowed producing mixed-matrix membranes to pursue enhancements of the RO performance, *e.g.* by using organic-inorganic and organic-bioorganic composite active layers (Lee et al., 2011).

In 2007 the first thin-film nanocomposite (TFN) RO membrane was introduced (Jeong et al., 2007). This nanotechnology-enhanced TFC featured a nanocomposite thin layer (<0.2 nm) produced by addition of zeolite nanoparticles during interfacial polymerisation of amino and acid chloride monomers. Zeolites are super-hydrophilic and negatively charged minerals which exhibit a 3-D pore network structure. This network serves as a sieve and it is claimed to provide a preferential flow path for water molecules (Jeong et al., 2007; Lind et al., 2009). Nanocomposite RO membranes have been reported to exhibit higher hydrophilicity and greater permeability, while exhibiting salt rejection comparable to that of a TFC (Hofs et al., 2013; Jeong et al., 2007; Lau et al., 2015; Lind et al., 2009; Pendergast et al., 2013). A variety of nanomaterials have been used to manufacture more permeable and fouling-resistant TFN RO membranes, *e.g.* titanium dioxide (Kwak et al., 2001), silver nanoparticles (Ben-Sasson et al., 2014) and carbon nanotubes (Vatanpour et al., 2017). These and other nanomaterials used in TFN membranes to enhance the overall performance are discussed in detail elsewhere (Lau et al., 2015; Lee et al., 2011).

In the last decade there has been a growing interest in biomimetic materials for water purification, particularly in aquaporin-embedded membranes. Aquaporins are a family of integral membrane proteins found in all three kingdoms of life at cellular level. These proteins form a pore structure that allows transport of water molecules driven by an osmotic gradient across biological membranes, while rejecting ionic solutes (Agre, 2004; Agre et al.,

1993). Kumar et al. showed that recombinant aquaporin AqpZ from a strain of *E. coli* remained active when incorporated in lipid vesicles and displayed permeability higher by more than one order of magnitude compared to TFC RO membranes, highlighting the potential benefits of developing biomimetic membranes for water treatment (Kumar et al., 2007). After less than a decade, mixed-matrix composite membranes with an organic-bioorganic active layer have been successfully manufactured and marketed. Several studies claimed that aquaporin-embedded RO membranes could outperform TFCs in terms of water permeability and selectivity while providing comparable salt rejection in bench-scale filtration tests (Li et al., 2015; Qi et al., 2016; Shen et al., 2014; Tang et al., 2013; Zhao et al., 2012).

To verify whether novel mixed-matrix membrane chemistry can outperform TFC chemistry regarding the removal of organic solutes, we investigated a set of 30 persistent polar MPs in RO filtration with nanocomposite and biomimetic membranes. A TFN membrane was tested with a pilot-scale RO system, where filtration was applied to a raw riverbank filtrate. Its performance was compared to that of a benchmark TFC membrane. To the best of our knowledge this is the first study in which a commercially available TFN was used in stand-alone RO applied to a natural water in pilot-scale drinking water treatment. Additionally, we characterised water permeability, salt rejection and organic solute passage through an aquaporin-based biomimetic membrane in a bench-scale RO filtration. The aquaporin RO membrane performance was compared to that of a benchmark TFC. No previous studies have attempted quantifying the passage of an extended set of polar MPs through biomimetic RO membranes. The filtration experiments with aquaporin RO membrane included two novel pollutants, *i.e.* trifluoromethanesulfonic acid (TFMSA) and 2-(Heptafluoropropoxy)-2,3,3,3-tetrafluoropropionic acid (HFPO-DA). These chemicals are emerging contaminants with high societal relevance. TFMSA, a super acid used in industrial applications, was only recently reported as ubiquitous water cycle contaminant (Zahn et al., 2016). HFPO-DA, a chemical introduced to replace perfluorooctanoic acid after it was found to be persistent, bioaccumulative and toxic (Kudo and Kawashima, 2003), was recently confirmed to occur in surface water impacted by wastewater from fluorinated chemical manufacturing and in drinking water produced from it (Gebbink et al., 2017; Versteegh and de Voogt, 2017). Besides being novel in terms of recent discovery in the aquatic environment, both TFMSA and HFPO-DA have not yet been investigated in RO filtration.

4.2. MATERIALS AND METHODS

4.2.1. Standards and chemicals

All chemicals used for this work were of analytical grade. More details are provided in the Appendix C (C-1). The model polar MPs tested in this study were chosen from scientific literature data using the following selection criteria: amenability for liquid chromatography-mass spectrometry analysis, detection in natural source waters, in finished drinking water and RO permeates. The target MPs selection is described is section 3.2.2 and elsewhere (Albergamo et al., 2019). The list of the polar MPs is shown in Table 4.1.

Table 4.1. List of model polar MPs and their physicochemical properties

Compound	Molecular weight (Da)	[a] p*K*a (pKb)	[a] log*D* (pH7)	Charge	Chemical classification
1H-benzotriazole	119.05	8.6	1.3	Neutral	Industrial chemical
2,6-dichlorobenzamide	188.97	12.1	2	Neutral	Biodegradation product
6-hydroxyquinoline	145.06	10.6	1.8	Neutral	Biodegradation product
Atrazine	215.09	15.8	2.2	Neutral	Herbicide
Barbital	184.19	7.5	0.6	Neutral	Pharmaceutical
Bisphenol A	228.29	9.8	4	Neutral	Personal care product
Caffeine	194.19	(-1.2)	-0.5	Neutral	Stimulant
Carbamazepine	236.27	16	2.8	Neutral	Pharmaceutical
Chloridazon	221.04	(-1.8)	1.1	Neutral	Herbicide
DEET	191.13	(-0.9)	2.5	Neutral	Herbicide
Diuron	233.09	13.2	2.5	Neutral	Herbicide
Diglyme	134.18	n/a	-0.32	Neutral	Industrial chemical
Paracetamol	151.16	0.4	1.2	Neutral	Pharmaceutical
Phenazone	188.22	(-0.5)	0.9	Neutral	Pharmaceutical
Phenylurea	136.06	13.8	0.9	Neutral	Industrial chemical
Tolyltriazole	133.15	8.8	1.8	Neutral	Industrial chemical
Triethyl phosphate	182.15	n/a	1.2	Neutral	Industrial chemical
Acesulfame	162.39	3	-1.5	Negative	Sweetener
Bentazon	240.28	3.7	-0.2	Negative	Herbicide
Diclofenac	295.02	4	1.4	Negative	Pharmaceutical
HFPO-DA*	330.05	3.8	1.34	Negative	Industrial chemical
PFBA	213.99	1.2	-1.2	Negative	Industrial chemical
PFBS	299.95	-3.3	0.2	Negative	Industrial chemical
PFOA	413.97	-4.2	1.6	Negative	Industrial chemical
Sulfamethazine	278.08	7	0.4	Negative	Pharmaceutical
Sulfamethoxazole	253.05	6.2	0.1	Negative	Pharmaceutical
TFMSA*	150.08	-3.43	-1.35	Negative	Industrial chemical

Table 4.1 (continued). List of model polar MPs and their physicochemical properties

Compound	Molecular weight (Da)	[a] pKa (pKb)	[a] log*D* (pH7)	Charge	Chemical classification
2-(methylamino)pyridine	108.07	(6.6)	0.7	Positive	Industrial chemical
Tetrabutylammonium	242.46	n/a	1.3	Positive	Industrial chemical
Tetrapropylammonium	186.35	n/a	-0.4	Positive	Industrial chemical

[a] p*K*a, p*K*b and log *D* calculated with Chemaxon (http://www.chemicalize.com); * Tested only with 1.8-inch modules (aquaporin-embedded and TFC RO membranes).

4.2.1.1. 4-inch modules

For the pilot-scale filtration experiments, the low-pressure RO (LPRO) membrane ESPA2-LD-4040 (Hydranautics) was chosen. The ESPA2 is a TFC with an active layer of cross-linked aromatic polyamide, typically used for filtration of brackish water. This TFC membrane served as benchmark to assess the performance of a TFN membrane, *i.e.* the mixed-matrix QuantumFlux Qfx-BW75ES brackish water RO membrane (LG NanoH2O).

4.2.1.2. 1.8-inch modules

For the bench-scale filtration experiments, 1.8-inch modules were used. We tested the AQPRTW-1812/150, a biomimetic RO membrane with a PA active layer embedded with aquaporin water channels (Aquaporin A/S), and a TW30-1812-100 (DOW Filmtech), the latter serving as a benchmark membrane for under-the-tap RO applications.

4.2.2. RO filtration systems

4.2.2.1. Hypoxic RO pilot (4-inch)

A pilot-scale RO system capable of keeping hypoxic conditions during filtration was used to investigate the removal of polar MPs from a raw riverbank filtrate by 4-inch TFN and TFC membranes. The membranes were tested in a separate run by applying the same filtration protocol. These experiments were conducted within the premises of a drinking water treatment plant in order to use an actual raw source water as RO feed water, *i.e.* anaerobic riverbank filtrate. This RO system was recently introduced by our research group and is described in Chapter 3 and in the literature (Albergamo et al., 2019). Briefly, the RO pilot consisted of an airtight stainless steel feed water reservoir (720 L) connected to a nitrogen supply, an immersed stainless steel coil fed with cooling liquid from a Hyfra Chilly 35 AC (by Krunkel), a high-pressure pump with frequency-controlled high-speed motor (DPVSV 2/26 B by DP-Pumps) and one 4-inch membrane pressure vessel. The permeate and concentrate lines were recirculated to the feed reservoir. A schematic diagram of the pilot is given in Figure 4.1. The feed reservoir was filled with approximately 700 L of freshly abstracted anaerobic riverbank filtrate while being flushed with nitrogen. Quality parameters of the feed water measured before dosing the polar MPs are given in Appendix C (Table C-2). A 2-L concentrated solution of polar MPs was prepared as described elsewhere (Albergamo et al. 2019) and dosed to the feed water with a SMART Digital pump (by Grundfos B.V.), resulting in MPs concentration between 10 and 20 µg/L. RO filtration was carried out at a fixed 15% recovery and permeate flux was set to 25 L m^{-2} h^{-1}. The feed temperature was 14±0.2 °C and the pH was 7.0±0.2. Filtration was

conducted for 4d before taking feed and permeate samples at t=96h to ensure equilibration of solute-membrane affinity interactions and avoid overestimating the passage of moderately hydrophobic MPs (Kimura et al., 2003a; Verliefde et al., 2007b). The feed reservoir was supplied with nitrogen during sampling to minimise intrusion of atmospheric oxygen into the system, which would result in precipitation of the dissolved iron naturally occurring in the anaerobic bank filtrate and subsequent fouling of the RO membrane. Feed water and permeate samples (V = 200 mL; n = 3) were collected in 250 mL polypropylene bottles and frozen immediately on site.

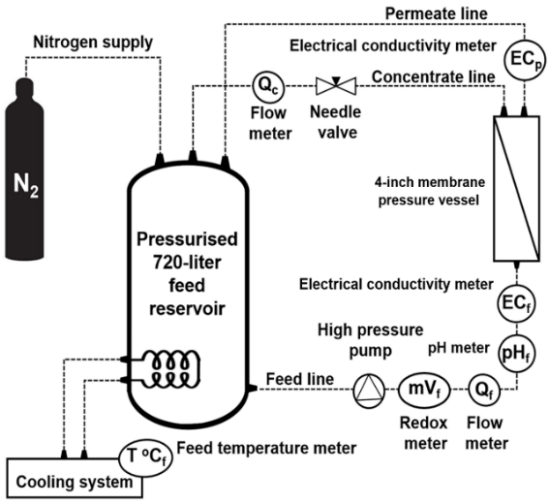

Figure 4.1. *Schematic diagram of the hypoxic RO pilot displaying the essential features of the system.*

4.2.2.2. Bench-scale RO (1.8-inch)

The bench-scale RO system consisted of a 500-L feed reservoir equipped with a chiller (FC1200, Julabo GmbH, Germany), a frequency controlled pump (DPVE2-30 by dp pumps Holland) and a concentrate valve to regulate the feed flow and pressure. Three parallel lines allowed simultaneous filtration with different RO membranes and recirculation of permeate and concentrate lines to the feed reservoir. The feed flow of each line was monitored by built-in rotamers. The feed pressure was monitored with a precision pressure gauge (WIKA 342.11.250 by Wika). The permeate flow was determined by weighing RO permeate collected in a glass cylinder over an exact time window of 30 sec. To investigate the removal of polar MPs by 1.8-inch aquaporin and TFC membranes the feed reservoir was filled with 400-L tap water previously filtered with Melt Blown 1 µm filters (by van

Borselen). A 20 mg/L polar MPs stock solution was dosed to the feed water to obtain the total MPs concentration of approximately 40 µg/L. Filtration was carried out by applying a feed pressure of 3 bar to obtain a permeate flux of 20 L m^{-2} h^{-1} at 5% recovery for both aquaporin and TFC RO membranes. The feed temperature was 17±0.2 °C and the pH was 6.2±0.1. Feed and permeate samples (V=50 mL; n=3) were collected into 50-mL polypropylene falcon tubes after 4 days and kept in the dark at 2 °C prior to analysis. A schematic diagram of the bench-scale RO system is shown in Figure 4.2.

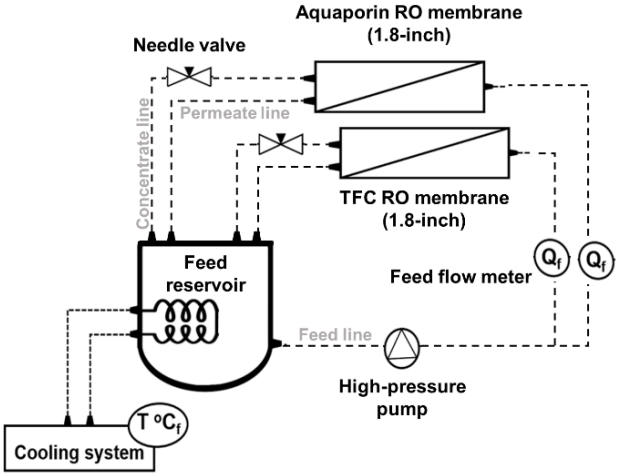

Figure 4.2. *Schematic diagram of the test bench RO displaying the essential features of the system.*

4.2.2.3. Characterisation of 1.8-inch RO membranes

The water permeability of the 1.8-inch aquaporin and TFC RO membranes was determined for deionised water (DI), DI with 1 g L^{-1} NaCl and tap water. The membranes were fitted in parallel pressure vessels and rinsed with demineralised water in one-pass operation for 20 min. The system was reverted to recirculation mode to carry out pure water permeability and salt passage tests. For pure water permeability, a feed pressure of 4 bar at a fixed feed flow of 160 L h^{-1} was applied. Measurements of feed and concentrate pressure as well as permeate flow were taken four times with 1h interval between each measurement. Further tests involved dosing 1 g L^{-1} of NaCl to the DI water and conducting RO filtration for 1h without changing operating conditions, *i.e.* with an applied feed pressure of 4 bar at a fixed feed flow of 160 L h^{-1}. For these tests, water permeability, salt passage (expressed as EC passage), and solute permeability were determined by

single measurements. Finally, DI was replaced with locally available low-DOC tap water as this was the feed type chosen to assess MPs passage. This tap water is produced from anaerobic groundwater, treated by aeration and rapid sand filtration and distributed without disinfectant residual. Filtration was carried out by applying a feed pressure of 3 bar at a feed flow of 160 L h^{-1} and the system was run for 94h. Water permeability was determined 1h after starting RO filtration and subsequently at t=48h, t=72h and t=96h. EC passage and solute permeability were instead quantified by single measurements at the beginning and at the end of the experiment, *i.e.* at t=1h and t=96h of RO filtration.

4.2.3. Chemical analysis

4.2.3.1. Inorganic analysis

Analysis of inorganics in the riverbank filtrate (feed water of hypoxic RO pilot) were performed by Vitens Laboratory (Utrecht, The Netherlands) via methods conforming to (inter)national standards. Feed water and RO permeate pH and electrical conductivity were analysed at KWR WaterCycle Research Institute (Nieuwegein, The Netherlands) with a Radiometer PHM210 and a Radiometer CDM83, respectively (both by Hach Lange BV).

4.2.3.2. Organic analysis

Aliquots of 1 mL feed water and RO permeate from samples taken as described in sections 2.3.1 and 2.3.2 for the pilot-scale and bench-scale RO, respectively, were spiked with a mixture of isotope-labelled internal standards to obtain a concentration of 2 µg/L. The aliquots were filtered with a 0.22 µm polypropylene filters (by Filter-Bio) and collected in 1.5 mL polypropylene vials. The samples were analysed by liquid chromatography high-resolution mass spectrometry (LC-HRMS) adopting a direct injection method validated for riverbank filtrate and surface water (Albergamo et al., 2018). The method relied on an ultrahigh-performance Nexera LC system (Shimadzu, Japan) equipped with a core-shell Kinetex biphenyl column with a particle size of 2.6 µm, inner diameter of 100 Å and dimensions of 100 x 2.1 mm column (by Phenomenex) for LC separation. The mobile phase eluents were DI 0.05% acetic acid (A) and methanol (B). A maXis 4G quadrupole time-of-flight HRMS (Bruker Daltonics) equipped with an electrospray ionisation source was operated in positive and negative mode to achieve MS detection. Unambiguous identification of the MPs was based on the mass accuracy of full-scan HRMS spectra and MS/MS spectra acquired in broadband collision induced dissociation mode (bbCID), retention time (t_R), isotopic it. In the Appendix C, the screening parameters for the model target analytes are provided (Table C-3.1), whereas the recoveries and limits of detection and quantification for direct injection

analysis of riverbank filtrate and RO permeate are provided in Table C-3.2. It is noteworthy that while a validation study for the analysis of tap water (bench-scale RO feed water) was not performed, the robustness and applicability of direct injection analysis to other water matrices has been previously shown (Albergamo et al., 2018). Hence, even if uncharacterised matrix effects may occur in tap water, the measurements of the bench-scale RO feed water (n=4) are considered reliable to compare the TFC and aquaporin RO membranes, which were fed in parallel in the bench-scale system. A separate chromatographic method was needed for the analysis of TFMSA. LC separation of TFMSA was achieved on an Acclaim Mixed-Mode WAX-1 column with a particle size of 3 µm, inner diameter of 120 Å and dimensions of 3.0 x 50 mm (Thermo Fisher). The mobile phase eluents were DI (A) and methanol (B), both 5 mM ammonium acetate. A 10-min linear gradient at 90% B and a flow of 0.3 mL/min were used. The sample injection volume was 80 ml.

4.2.4. Assessment of solute passage

The following equation was used to express the passage of solutes by RO membranes:

$$P\ (\%) = (C_{ROP}/C_{ROF}) \times 100 \quad (1)$$

where C_{ROP} and C_{ROF} are the concentrations in the permeate and the feed water, respectively.

The EC passage was calculated as:

$$EC\ P\ (\%) = (EC_{ROP}/EC_{ROF}) \times 100 \quad (2)$$

where EC_{ROP} and EC_{ROF} are the electrical conductivity (in µS/cm) in the permeate and the in the bulk feed solution, respectively.

Based on the solution-diffusion model the water permeability (A) of RO membranes was calculated by rearranging the permeate flux equation (Wang et al., 2014; Wijmans and Baker, 1995):

$$J_W = A\ (\Delta P - \Delta\Pi) \quad (3)$$

Where J_W is the permeate flux (in L m^{-2} h^{-1}), ΔP and $\Delta\Pi$ indicate the pressure and osmotic pressure difference across the membrane, respectively.

Similarly, the solute permeability (B) was calculated as:

$$B = J_w\ (C_{ROP} / C_{ROF} - C_{ROP}) \quad (4)$$

Finally, one-way analysis of variance (ANOVA) with 95% confidence interval was computed within the R statistical environment (version 3.4) (R Core Team, 2017). This analysis was performed with the purpose of assessing the statistical differences between the passage values quantified for the different membranes. Two ANOVA analyses were performed, one for pilot-scale and for one bench-scale RO filtration, respectively.

4.3. RESULTS AND DISCUSSION

4.3.1. Hypoxic pilot-scale RO performance (4-inch)

In a previous work conducted with the same RO system it was shown that the physicochemical properties of the compounds were significantly related to passage rate through TFC membranes. These properties were specifically size and charge, whereas hydrophobicity did not show statistical significance difference compared to hydrophilicity (Albergamo et al., 2019). Hence, based on these earlier findings and on other literature data, all neutral MPs are discussed together and separately from ionic MPs.

Samples to determine the passage of polar MPs were taken at the 5th day of filtration at a permeate flux of 25 L m^{-2} h^{-1} and 15% recovery. The stability of the hypoxic conditions of the feed water was assured by an online redox potential meter, which displayed negative values throughout the duration of the filtration experiments. At the moment of sampling, the TFN membrane displayed a water permeability of 1.22 L m^{-2} h^{-1} bar^{-1} and an EC passage of 1.2%, whereas the TFC showed a water permeability of 1.95 L m^{-2} h^{-1} bar^{-1} and an EC passage of 0.9%. At a fixed feed flow of ≈ 1 m^3 h^{-1} the TFN required a feed pressure of 19.55 bar to match the operating conditions, while the TFC needed 13.35 bar. This was not in line with literature data, which suggested higher water permeability of TFNs compared to TFCs membranes (cf. Chapter 4.1). A lower permeability of the TFN membrane due to compaction was ruled out, as zeolite-embedded polyamide active layers are reportedly less prone to undergo such modifications (Pendergast et al., 2013). Hofs et al. showed that a 4-inch seawater QuantumFlux TFN outperformed a benchmark TFC membrane in water permeability by a factor of 2 in pilot-scale RO applied to tap water with 1 g L^{-1} NaCl at a permeate flux of 15 L m^{-2} h^{-1} and 7% recovery (Hofs et al., 2013). That study found that the TFN was less hydrophilic compared to the TFC based on contact angle measurements. The TFN's lower permeability observed in our study might be supported by this finding. While Hofs et al. used filtered tap water, we used raw riverbank filtrate as RO feed water, which contained humic and fulvic acids in the low mg L^{-1} range. Therefore, it could be speculated that the higher affinity for humic and fulvic acids naturally occurring in the bank filtrate could have led to reduced water and solute permeability (Agenson and

Urase, 2007; Fujioka et al., 2013; Tang et al., 2007). However, flux decline data to support this statement are not available.

4.3.1.1. Removal of neutral MPs by hypoxic RO pilot (4-inch)

The removal of neutral MPs expressed as compound passage though the TFN and the benchmark TFC membranes is shown in Figure 4.3a. The passage of neutral polar MPs through 4-inch TFC and TFN membranes followed a similar pattern. The TFN, however, proved to be a more effective barrier against neutral polar MPs, for which passage values between 0.1% and 6.1% were quantified. These values ranged from 0.1% to 14.7% when filtration was carried out with the benchmark TFC. The TFN was more effective in rejecting neutral polar MPs with molecular weight below 150 Da and comparable to the TFC for larger neutral MPs. The only exception was the plasticiser bisphenol A, a neutral polar MPs having a log D_{pH7} of 4, thus exhibiting hydrophobic properties. Bisphenol A displayed 4.2±2.6% and 1.8±0.3% passage through the TFN and TFC RO membranes, respectively. Its incomplete removal by RO with low-pressure TFC membranes has been reported before in literature and it is thought to be caused by affinity interactions with the membrane active layer, ultimately enhancing the solution-diffusion mechanism (Kimura et al. 2004; Comerton et al. 2008). The higher passage of bisphenol A through the TFN could be supported by the higher hydrophobicity of the QuantumFlux nanocomposite as measured by Hofs et al. (Hofs et al. 2013). In order of size expressed as molecular weight, the smallest neutral polar MPs were 1H-benzotriazole (119.12 Da) < tolyltriazole (133. 15 Da) < 6-hydroxyquinoline (145.16 Da) < diglyme (134.17 Da) < phenylurea (136.15 Da) < 6-hydroxyquinoline (145.16 Da). As expected, the smallest neutral polar MP, 1H-benzotriazole, displayed the highest passage through TFC and TFN RO membranes with values of 14.7±1.7% and 6.1±1.1%, respectively. The second least-removed MP was tolyltriazole, which displayed passage values of 8.0±1.5% and 4.1±1.4% with the TFC and TFN RO membranes, respectively. The third least-removed MP was 6-hydroxyquinoline with passage values of 5.5±0.4% and 2.1±0.4% with the TFC and TFN RO membranes, respectively. Overall the passage-size pattern displayed by neutral polar MPs was in accordance with literature on removal of polar organic solutes by TFC (Fujioka et al., 2015a) and TFN RO membranes (Hofs et al., 2013). Hofs at al. investigated the removal of 8 neutral nitrosamines and 21 pharmaceuticals including neutral and ionic compounds by TFN and TFC membranes (Hofs et al. 2013). While both membranes achieved excellent rejections of pharmaceuticals (>99%), most nitrosamines were well rejected (>90%) according to their molecular weight. NDMA, the smallest nitrosamine with a molecular weight of 74.1 Da, was rejected for ≈ 62% and ≈ 74% by the TFN and the TFC RO membrane, respectively. This was partially in accordance with our results, as we also

observed a higher passage for the smallest neutral MPs, but in our case the TFN exhibited lower passage values. It is challenging to thoroughly compare our study to that of Hofs et al. as we used a raw natural water as RO feed, whereas they used filtered tap water, which is a much simpler matrix. Considering that similar removal patterns were exhibited by the 4-inch membrane modules tested with the RO-pilot, and that the TFN's nanoparticle load is estimated to be below 6 wt% (Hofs et al., 2013), it could be assumed that separation of organic solutes by nanocomposite active layers followed the solution-diffusion mechanism through PA for both membranes.

4.3.1.2. Removal of ionic MPs by hypoxic RO pilot (4-inch)

The passage of anionic MPs through TFN and TFC RO membranes is shown in Figure 4.3b. Excellent removal of negatively charged organic solutes was observed for both membranes and passage values lower than 1% were quantified in all cases. It could be assumed that both membranes would exhibit a negative charge at feed water pH due to deprotonation of acidic functional groups on the polyamide (nano)composite (Bellona et al., 2004; Lau et al., 2015; Ozaki and Li, 2002). Literature data supported this assumption as no zeta-potential differences were observed between a QuantumFlux TFN and a benchmark TFC RO membranes (Hofs et al., 2013). Electrostatic repulsion with negatively charged RO membranes prevents anionic MPs from dissolving into the active layer (Nghiem et al., 2006; Verliefde et al., 2008), representing a strong factor enhancing chemical removal by RO.

Good removal of cationic MPs was provided by both membranes tested with the hypoxic RO pilot, with passage values lower than 5% in all cases. The TFN proved to be a more effective barrier for the smallest cationic MP, *i.e.* 2-(methylamino)pyridine (109.08 Da), for which 2.3% passage was quantified against 4.3% displayed by the TFC. In this case, the better performance of the TFN could be explained by the cation exchange capacity of zeolites embedded in nanocomposite films (Loiola et al., 2012). 2-(methylamino)pyridine was the smallest compound investigated in this study, nevertheless it displayed lower passage than the second-smallest 1H-benzotriazole (119.12 Da), which was uncharged instead. This indicated that additional solute-membrane interactions, likely electrostatic, prevent small cationic MPs to dissolve and diffuse through negatively charged (nano)composite resulting in a lower passage compared to neutral MPs of similar size. The organic ammonium cations were slightly better removed by the TFC, nevertheless in all cases passage values lower than 0.5% were quantified for tetrapropylammonium and tetrabutylammonium (0.4 % and 0.1% passage with both membranes). For these compounds, electrostatic

sorption, Donnan exclusion and size exclusion are expected to play a role in restraining chemical mobility through the RO membranes.

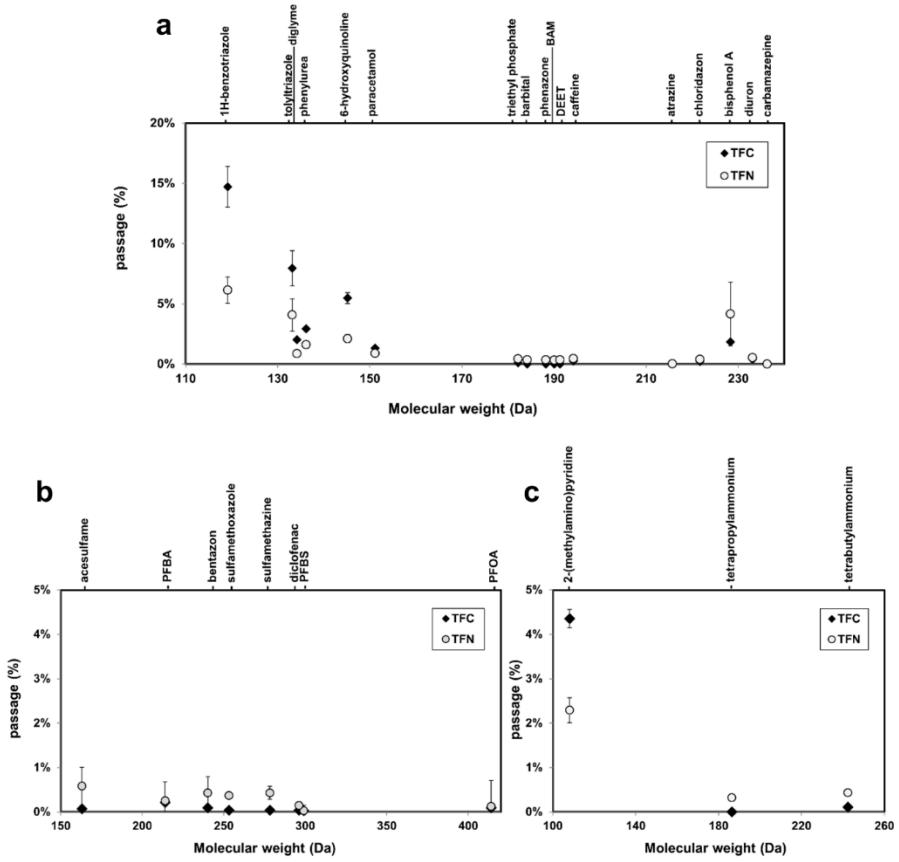

Figure 4.3. *Passage of neutral polar MPs (a), anionic MPs (b) and cationic MPs (c) through TFN and TFC as a function of compound molecular weight. Error bars are shown when larger than the data point symbol and indicate the standard deviation of the measurements for n=3 samples. Conditions: average permeate flux 25 L m^{-2} h^{-1}, recovery 15%, feed pH 7.0±0.2, feed conductivity 973±7 µS/cm, feed temperature 14±0.2 °C.*

4.3.1.3. Statistical validation of pilot-scale RO results (4-inch)

The passage data of the model MPs quantified in pilot-scale RO filtration were combined, log-transformed and visualised as box-and-whisker plots. These results are shown in Figure 4.4. It can be seen that when pilot-scale RO filtration was carried with the ESPA2, which was the reference TFC, the

log-passage displayed by the polar MPs exhibited a slightly larger range compared to that of the TFN. Nevertheless, the median log-passage measured for the two membranes (black lines within each box) were quite comparable, suggesting that no major differences were observed between the TFC and the TFN membranes. The ANOVA assessment returned an *F*-value of 0.424 and a *p*-value of 0.518 with a 95% confidence interval. This confirmed that there were no significant differences between the TFN and the benchmark TFC RO membranes.

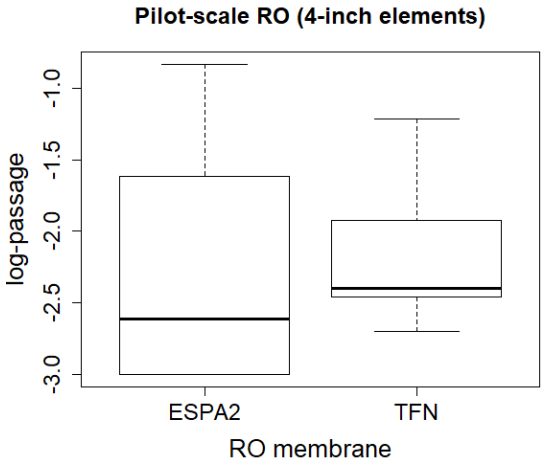

Figure 4.4. *Box-and-whisker plot illustrating the log-passage ranges quantified for 28 polar MPs during filtration with thin-film composite (ESPA2) and thin-film nanocomposite (TFN) RO membranes.*

4.3.2. Bench-scale RO (1.8-inch)

4.3.2.1. Aquaporin and TFC RO membranes performance

Water permeability and salt passage of the 1.8-inch aquaporin and benchmark TFC RO membranes were determined in the bench-scale RO system. The performance data are presented in Table 4.2. When deionised water was used as feed water, the aquaporin membrane was more permeable than the TFC by 33-35%. The higher permeability of the aquaporin membrane ($A_{aquaporin}$ = 10.22±0.03 L m^{-2} h^{-1} bar^{-1}) compared to that of the benchmark TFC membrane (A_{TFC} = 7.63±0.12 L m^{-2} h^{-1} bar^{-1}) might result from the water-selective protein channels embedded in the bioorganic composite, although a less dense membrane structure could not be ruled out. Upon checking the stability of the filtration performance over 4h, NaCl was added to the DI water to a concentration of 1g L^{-1}. In these conditions,

water permeability of the aquaporin membrane decreased by 37%, whereas the TFC membrane displayed a decrease of 26%. In biological systems, comparable levels of salinity result in the closure of the aquaporin protein water channels (Henzler et al., 2004), which could potentially explain the reduction in water permeability of the aquaporin membrane. The TFC displayed salt passage and solute permeability (B) higher than those of the aquaporin membrane by nearly a factor of 2 while exhibiting half of the trade-off value (A/B). This indicated the higher permeability of the aquaporin RO membrane to water molecules and lower selectivity for monovalent ions in high salinity conditions. No substantial differences in the evaluated performance parameters were observed between the aquaporin and TFC membranes over 96h of RO filtration when tap water was used as feed water. In addition, the two membranes displayed a comparable flux decline over time, as shown in Figure 4.5.

Table 4.2. Performance of aquaporin-embedded and benchmark TFC RO membranes (1.8-inch).

		Water permeability (A)	**Salt passage**	**Solute permeability (B)**	**Trade-off (A/B)**
		L m^{-2} h^{-1} bar^{-1}	%	L m^{-2} h^{-1}	bar^{-1}
Aquaporin	[a] DI	10.22±0.03	N/A	N/A	N/A
	[b] DI + NaCl 1g/L	6.34	7.01	1.89	3.35
	Tap water	[c] 5.43±1.37	[d] 2.4±0.4	[d] 0.39±0.19	13.92
TFC	[a] DI	[a] 7.63±0.12	N/A	N/A	N/A
	[b] DI + NaCl 1g/L	[b] 5.39	15.52	3.96	1.36
	Tap water	[c] 5.10±0.94	[d] 2.4±1.1	[d] 0.39±0.23	13.07

[a] n=4 (one measurement per hour, value after the ± sign indicates standard deviation of the measurements), feed pressure = 4 bar; [b] n =1, feed pressure = 4 bar; [c] n=4 (measured at t=1h, t= 48h, t=72h and t=96h. Value after the ± sign indicates standard deviation of the measurements) and feed pressure = 3 bar; [d] n=2 (average of measurements taken at t=1h and t = 96h, value after the ± sign indicates the range of the duplicates); N/A = not available.

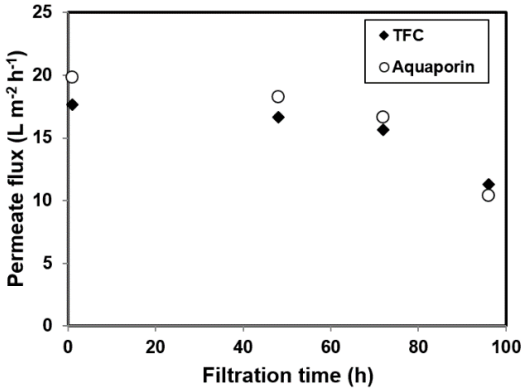

Figure 4.5. *Flux decline expressed as permeate flux over time (h) of the aquaporin and TFC RO membranes in bench-scale filtration.*

4.3.2.2. Removal of neutral MPs in bench-scale RO (1.8-inch)

The passage of neutral MPs through aquaporin and benchmark TFC RO membranes is shown in Figure 4.6a. The order in which the neutral MPs were removed by the 1.8-inch membranes was similar to that observed in pilot-scale RO filtration, although the passage of uncharged polar MPs smaller than 150 Da was higher in bench-scale. For example, while 1H-benzotriazole displayed 14.7±1.7% with the 4-inch TFC membrane, values of 44±4% and 65±10% were quantified for the 1.8-inch TFC and the aquaporin RO membranes, respectively. As feed water pH and temperature did not differ substantially between bench-scale (pH 6.2±0.1, T=17 °C) and pilot-scale (pH 7.0±0.2, T=14±0.2 °C), the higher passage of neutral MPs and the higher water permeability of the 1.8-inch might result from a more open structure compared to the 4-inch RO membranes.

In bench-scale filtration, neutral MPs smaller than 150 Da exhibited higher passage through the aquaporin membrane compared to the TFC membrane. The passage of the five smallest neutral MPs, *i.e.* 1H-benzotriazole (119,12 Da), tolyltriazole (133.15 Da), diglyme (134.18 Da), phenylurea (136.15 Da) and 6-hydroxyquinoline (145.16 Da) ranged according to size from 44±4% to 19±1% with the TFC membrane, whereas the range for the aquaporin membrane was 65±10% to 30±5%. No differences were observed for larger compounds. Despite evidence of diffusion of small neutral organics and even small peptides through aquaporin water channels exists (Henzler et al., 2004; Kocsis et al., 2018; Uehlein et al., 2007), MPs passage is believed to mostly occur through the PA active layer. This was recently confirmed for aquaporin-embedded PA forward osmosis membranes (Xie et al., 2018). Unfortunately,

further RO studies to compare the results of the aquaporin membrane were not found in the literature.

4.3.2.3. Removal of ionic MPs in bench-scale RO (1.8-inch)

The passage of ionic MPs through the biomimetic aquaporin and a benchmark TFC is shown in Figure 4.6b (anionic) and Figure 4.6c (cationic). Variations due to different concentration polarisation conditions were not expected as membrane modules of the same size were used (Verliefde et al., 2008) and the operating conditions were similar during the experiments.

Anionic MPs were extremely well removed and exhibited passage values lower than 1% in all cases with both membranes, except PFBS, which displayed 4% passage with both aquaporin and TFC membranes. In all cases the quantification limits were used as permeate concentrations, leading to overlapping data points in Figure 4.6b. In the present study the passage of TFMSA in RO filtration was quantified for the first time. The dedicated method required to analyse TFMSA was not validated due to time constraints. Nevertheless, its output was considered reliable on the basis of linearity of the calibration series used for quantification (R^2=0.9986) and on the standard error of the measured samples (<13%). TFMSA displayed passage of 0.4% with both membranes, indicating that under-the-tap RO modules (1.8-inch) perform as well as the 4-inch membranes in retaining small anionic MPs.

As for cationic MPs (Fig. 4.6c), the ammonium cations displayed less than 1.5% passage through both aquaporin and TFC RO membranes. Surprisingly, the smallest cation 2-(methylamino)pyridine displayed passage comparable to that of 1H-benzotriazole with both aquaporin and TFC RO membranes. This data did not reflect what was observed in the hypoxic RO pilot, where negatively charged DOC naturally occurring in the bank filtrate (pilot-scale RO feed water) might have possibly decreased the passage of small cations further. A lesser charge of the 1.8-inch modules compared to the 4-inch modules could also explain this phenomenon, however supporting zeta-potential measurements of the modules used in this study were not available nor found in literature.

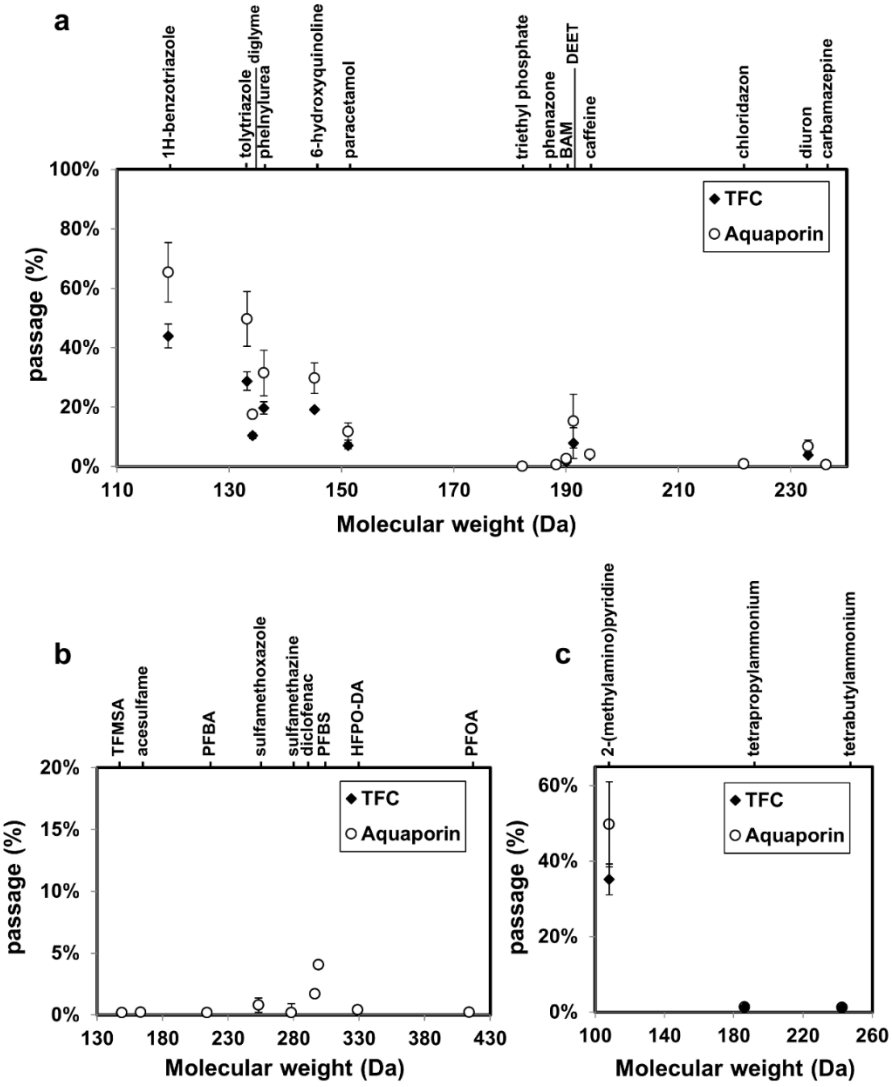

Figure 4.6. *Passage of neutral polar MPs (a), anionic MPs (b) and cationic MPs (c) through 1.8-inch aquaporin and TFC RO membranes as a function of compound molecular weight. Error bars are shown when larger than the data point symbol and indicate the standard deviation of the measurements for n=3 samples. Conditions: average permeate flux 20 L m^{-2} h^{-1}, recovery 6%, feed pH 6.2 ±0.1, feed conductivity 237 µS/cm, feed temperature 17 °C.*

4.3.2.4. Statistical validation of bench-scale RO results (1.8-inch)

The passage values quantified for the model MPs in bench-scale RO filtration were treated as done for the pilot-scale dataset, *i.e.* the data were combined, log-transformed and visualised as box-and-whisker plots. The results are shown in Figure 4.7. The log-passage ranges and median log-passage determined for the polar MPs were highly comparable for the two membranes. The ANOVA to validate this observation returned an *F*-value of 0.153 and a *p*-value of 0.697 with a 95% confidence interval. This indicated that there was no significant difference between the aquaporin and benchmark TFC RO membranes.

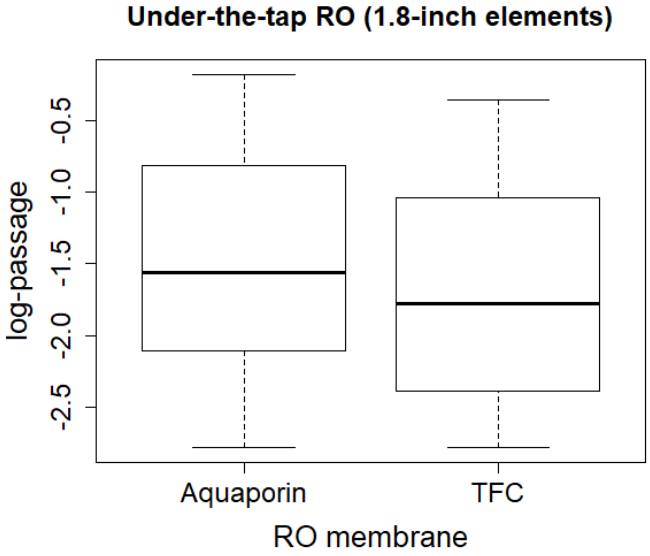

Figure 4.7. *Box-and-whisker plot illustrating the log-passage ranges quantified for 28 polar MPs during filtration with thin-film composite (TFN) and biomimetic (Aquaporin) RO membranes.*

4.4. CONCLUSIONS

In pilot-scale RO filtration applied to a natural water, the overall differences in MPs passage between a 4-inch TFN and a TFC were not significant. Nevertheless, these following conclusions were made:

- The TFN was a more effective barrier against neutral polar MPs smaller than 150 Da and comparable for larger molecules. The passage differences between the two membranes became narrower with increasing MPs molecular weight. This indicated that neutral polar MPs are mostly removed according to their size and that the zeolite

nanoparticles embedded in the nanocomposite active layer might act as additional sieves.

- Anionic MPs were extremely well removed by both TFC and TFN membranes, indicating that electrostatic repulsion prevented diffusion of these chemicals in polyamide-based RO membranes regardless of the presence of embedded additives. Cationic MPs were also well removed by both membranes, although the TFN displayed lower passage of the smallest cation. For the three cationic MPs, passage was lower than that of neutral MPs of comparable size, indicating a substantial contribution of electrostatic interaction in preventing diffusion of small cations to the permeate side.

In bench-scale RO filtration applied to tap water, the overall differences in MPs passage between a 1.8-inch aquaporin-embedded RO membrane and a TFC were not significant. Nevertheless, these following conclusions were made:

- The aquaporin-embedded RO membrane for under-the-tap applications was more water-permeable and exhibited a lower EC passage than the benchmark TFC when deionise water was used as feed water, suggesting both higher affinity for water molecules and less affinity for salts. When tap water was used as feed water, higher water permeability resulted in higher organic solute passage as shown by the permeability-selectivity trade-off, highlighting the different behaviour of salts from that of organics.

- Anionic MPs were extremely well removed by the 1.8-inch modules, proving the robustness of RO for anionic organics. On the other hand, small cationic MPs were more problematic with the 1.8-inch modules regardless of membrane chemistry.

Our study indicated that while different active layer chemistry can result in different passage values of organic solutes, commercially available nanocomposite and biomimetic RO membranes cannot yet significantly outperform benchmark TFCs. More research on membrane materials is needed to improve the performance of RO against polar MPs and overcome the limitations posed by the permeability-selectivity relationship trade-off.

ACKNOWLEDGMENTS

This study was conducted with the ECROS project and was funded by the drinking water company Oasen (Gouda, The Netherlands). Aquaporin A/S (Kongens Lyngby, Denmark) is greatly acknowledged for donating the 1.8-inch biomimetic RO membrane module. Harmen van der Laan, Evgeni Alaminov, Behailu Wolde, Eva Kocbek and Chris Bierman, are acknowledge for assistance with the RO pilot filtration experiments at Oasen. Willem-Jan Knibbe at Wageningen University (The Netherlands) is acknowledged for helpful discussions about the results obtained in this study. Daniel Zahn and Thomas Knepper from the University of Applied Science Fresenius (Idstein, Germany) are acknowledged for donating the TFMSA analytical standard. Rick Helmus is acknowledged for support with setting up the analytical method for TFMSA. Danny Harmsen is acknowledged for assisting with setting up the bench-scale RO system at KWR and for performing the pH measurements.

APPENDIX C. Supplementary information to Chapter 4

C-1. STANDARDS AND CHEMICALS

Analytical grade unlabelled standards (purity >95%) of 1H-benzotriazole, 2-(methylamino)pyridine, 2,3,3,3-Tetrafluoro-2-(1,1,2,2,3,3,3-heptafluoropropoxy)propanoic acid (HFPO-DA), 2,6-dichlorobenzamide (BAM), 4-methyl-1H-benzotriazole (tolyltriazole), 6-hydroxyquinoline, acesulfame, atrazine, barbital, bentazon, bisphenol A, caffeine, carbamazepine, chloridazon, *N,N-D*iethyl-meta-toluamide (DEET), diclofenac, diuron, diglyme, ibuprofen, paracetamol, perfluorobutyric acid (PFBA), perfluorooctanoic acid (PFOA), perfluorobutanesulfonic acid (PFBS), phenazone, phenyl urea, sulfamethazine, sulfamethoxazole, tetrabutylammonium, tetrapropylammonium and triethyl phosphate were purchased from Sigma-Aldrich (Zwijndrecht, The Netherlands).Trifluoromethanesulfonic acid (TFMSA) from Sigma-Aldrich (Schnelldorf, Germany) was donated by the Institute for Analytical Research (IFAR), University of Applied Science Fresenius (Idstein, Germany). The isotope-labelled standards, 1H-benzotriazole-d4, atrazine-d5, bisphenol A-d16, caffeine-13C3, carbamazepine-13C6, diclofenac-13C6, diuron-d6, ibuprofen-d3, paracetamol-d4, and sulfamethoxazole-13C6 were purchased from Sigma-Aldrich (Zwijndrecht, The Netherlands), whereas DEET-d6, sulfamethazine-13C6, triclosan-13C6, and triethyl phosphate-d15 were purchased from Cambridge Isotope Laboratories Inc. (Andover, MA, USA). In-house deionised water was purified with an ELGA water purification system (Veolia Water Technologies Netherlands B.V., Ede, the Netherlands). Analytical grade (LC-MS) methanol (MeOH) was purchased from Biosolve (Valkenswaard, The Netherlands), acetic acid were purchased by Merck (Damstadt, Germany).

Table C-2. Quality parameters of the riverbank filtrate dosed in the feed reservoir of the pilot-scale RO system (measured prior to dosing organic micropollutants)

Parameter	Unit	Value
pH	-log[H^+]	7.1
Temperature	°C	14.2
EC at 20 °C	µS/cm	935
Redox potential	mV	-63
Sodium	mg/l	98.9
Potassium	mg/l	5.1
Calcium	mg/l	100
Magnesium	mg/l	16.7
Iron	mg/l	0.044
Manganese	mg/l	0.386
Hydrogen carbonate	mg/l	322
Hardness	mmol/l	3.18
Chloride	mg/l	120
Ammonium	mg/l	1.97
Phosphate	mg/l	<0,03
Sulphate	mg/l	100

C-3. UHPLC-ESI-q-ToF/HRMS screening parameters and performance

Table C-3.1. Target MPs monitored ions, chromatographic retention times, assigned internal standards, qualifier ion ratios

Compound	Formula	Quantifier m/z (Q)	t_R (min)	ESI mode	Internal standard	Qualifier m/z (q)	q/Q
1H-benzotriazole	C6H5N3	120.0556	4.3	+	1H-benzotriazole-D4	92.049	0.1
2-(methylamino)pyridine	C6H8N2	109.0760	3.1	+	n/a	78.0332	0.15
5-methyl-1H-benzotriazole	C7H7N3	134.0713	4.8	+	1H-benzotriazole-D4	92.049	0.15
6-hydroxyquinoline	C9H7NO	146.0600	4.0	+	Quinoline-D7	118.0651	0.2
Acesulfame	C4H4HNO4S	161.9867	2.9	-	n/a	82.0294	0.2
Antipyrine	C11H12N2O	189.1022	5.1	+	Atrazine-D5	174.0788	0.05
Atrazine	C8H14ClN5	216.1011	5.5	+	Atrazine-D5	174.0543	0.5
BAM	C7H5Cl2NO	189.9821	4.5	+	Caffeine-13C3	174.9527	0.6
Barbital	C8H12N2O3	183.0775	4.3	-	n/a	140.071	0.05
Bentazon	C10H12N2O3S	239.0496	5.1	-	n/a	132.0324	0.15
Bisphenol A	C15H16O2	227.1078	5.5	-	Bisphenol A-d16	287.1289	0.1
Caffeine	C8H10N4O2	195.0877	4.8	+	Caffeine-13C3	138.0664	0.5
Carbamazepine	C15H12N2O	237.1022	5.7	+	Carbamazepine-13C6	192.0812	0.2
Chloridazon	C10H8ClN3O	222.0429	4.9	+	Diuron-d6	104.0494	0.15
DEET	C12H17NO	192.1383	5.8	+	DEET-D6	91.0538	0.1
Diclofenac	C14H11Cl2NO2	294.0094	6.2	-	Diclofenac-13C6	250.0188	0.7
Diglyme	C6H14O3	135.1016	4.1	+	n/a	152.1281	0.5
Diuron	C9H10Cl2N2O	233.0243	5.5	+	Diuron-d6	218.0981	0.4
HFPO-DA	C6HF11O3	328.9677	4.7	-	n/a	284.9782	0.35
Ibuprofen	C13H18O2	205.1234	6.0	-	Ibuprofen-D3	161.133	0.15
Paracetamol	C8H9NO2	152.0706	3.3	+	Paracetamol-D4	110.0601	0.3
PFBA	C4HF7O2	212.9792	3.1	-	n/a	168.9889	0.1
PFOA	C8HF15O2	412.9664	5.3	-	n/a	368.9749	0.5
PFBS	C4HF9O3S	298.9430	4.4	-	n/a	79.9569	0.04
Phenyl urea	C7H8N2O	137.0709	4.0	+	Paracetamol-D4	94.0648	0.08
Sulfamethazine	C12H14N4O2S	279.091	4.9	+	Sulfamethazine-13C6	156.0116	0.25

Table C-3.1 (continued). Target MPs monitored ions, chromatographic retention times, assigned internal standards, qualifier ion ratios

Compound	Formula	Quantifier m/z (Q)	t_R (min)	ESI mode	Internal standard	Qualifier m/z (q)	q/Q
Sulfamethoxazole	C10H11N3O3S	254.0594	4.7	+	Sulphamethoxazole-13C6	156.0116	0.35
Triethyl phosphate	C6H15O4P	183.0781	5.1	+	TEP-D15	98.9838	0.9
Tetrabutylammonium	C16H36N	242.2842	5.4	+	Quinoline-D7	142.1593	0.25
Tetrapropylammonium	C12H28N	186.2216	4.4	+	Quinoline-D7	114.1279	0.4
TFMSA [a]	CF3SO3H	148.9519	7.3	-	n/a	79.9569	n/a

[a] Required dedicated chromatographic method with mixed-mode weak anion exchange stationary phase. Details in section 4.3.2.1.

Table C-3.2. Direct injection method recoveries, limits of detection and quantification in riverbank filtrate and RO permeate.

Compound	Riverbank filtrate			RO permeate [a]		
	Recovery	LOQ	LOD	Recovery	LOQ	LOD
	(%±SD)	ng/L	ng/L	%±SD	ng/L	ng/L
1H-benzotriazole	93±16	63	19	113±9	63	19
2-(methylamino)pyridine	83±13	26	8	112±18	35	11
BAM	110±7	125	38	102±13	64	19
6-hydroxyquinoline	78±15	63	19	85±7	31	9
Acesulfame	128±39	117	35	102±19	63	19
Atrazine	95±7	31	9	96±10	31	9
Barbital	66±8	276	83	104±8	60	18
Bentazon	102±18	269	76	94±3	30	9
Bisphenol A	96±13	250	76	108±12	125	38
Caffeine	96±14	63	19	104±11	63	19
Carbamazepine	108±29	63	19	107±17	63	19
Chloridazon	91±16	31	9	106±13	31	9
DEET	97±12	31	9	103±16	31	9
Diclofenac	109±24	63	19	97±10	31	9
Diglyme	86±3	15	53	108±11	68	20
Diuron	99±6	31	9	96±10	31	9
HFPO-DA	89±15	59	19	92±16	39	9
Paracetamol	93±12	63	19	105±13	63	19
PFBA	79±47	133	9	113±18	125	38
PFBS	109±33 [b]	125 [b]	38 [b]	110±19	114	34
PFOA	106±17	56	19	96±13	33	10
Phenazone	106±15	63	19	102±10	31	9
Phenylurea	81±31	63	19	100±13	63	19
Sulfamethazine	91±25	31	9	94±15	31	9
Sulfamethoxazole	90±6	31	9	90±13	31	9
Tetrabutylammonium	95±10	31	9	96±9	31	9
Tetrapropylammonium	103±12	31	9	81±7	31	9
Tolyltriazole	92±8	31	9	102±13	63	19
Triethyl phosphate	93±13	31	9	104±14	31	9
TFMSA [c]	N/A	N/A	N/A	N/A	63 [c]	19 [c]

LOQ: Limit of quantification; LOD: Limit of detection; [a] Calculated by testing 4 replicates in one day (except for TFMSA, see footnote "c"); [b] Calculated by testing 3 replicates in one day; [c] Value derived from a calibration series prepared following the procedure described in Chapter 2.2.5 and complying with the criteria set therein.